# **Effects of Multiple Pulses on Nanosecond Discharges**

Alfredo Duarte Gomez\*, Nicholas Deak †, Fabrizio Bisetti<sup>‡</sup> *The University of Texas at Austin, Austin, Texas, 78712* 

Numerical simulations of axisymmetric nanosecond pulsed discharges at atmospheric pressure and temperature are performed with a novel fully implicit time integration approach. The plasma fluid equations with a drift-diffusion model and local-field approximation are made dimensionless and solved using a preconditioned Jacobian Free Newton-Krylov method. A simplified kinetics model is employed, including electrons, one positive ion, and one negative ion. The chemical processes of ionization, attachment, detachment, and recombination are considered along with photoionization. The newly developed fully-implicit integration scheme with physics-based preconditioning allows for the efficient simulations capable of describing the cathode sheath over time-scales of  $O(10~\mu s)$ . The implicit solver overcomes the limiting time scales related to electron drift, diffusion, dielectric relaxation, and ionization.

#### I. Nomenclature

n = dimensionless electron number density

u = dimensionless positive ion number density

v = dimensionless negative ion number density

 $\rho$  = dimensionless space charge

 $\theta$  = dimensionless electric field

 $\varphi$  = dimensionless electric potential associated with space charge

 $a_i$  = dimensionless model constants

 $\alpha_0$  = reference degree of ionization  $\tilde{n}_0/\tilde{N}$ 

 $\omega$  = dimensionless chemical source term

 $T_e$  = dimensionless electron temperature

T = dimensionless gas temperature

 $\tilde{e}$  = unit charge (C)

 $\tilde{\lambda}_0$  = reference Debye length (m)

 $\tilde{\omega}_0$  = reference plasma frequency (s<sup>-1</sup>)

 $\tilde{n}_0$  = reference number density (m<sup>-3</sup>)

 $\tilde{T}_0$  = reference temperature (K)

 $\tilde{\mu}_{e,i}$  = electron and ion mobilities (m<sup>2</sup> V<sup>-1</sup> s<sup>-1</sup>)

 $\tilde{\epsilon}_0$  = vacuum permitivity (F m<sup>-1</sup>)

 $\tilde{T}_B$  = background gas temperature (K)

 $\tilde{N}_B$  = background gas number density (m<sup>-3</sup>)

 $\tilde{k}_B$  = Boltzmann constant (J K<sup>-1</sup>)

 $\tilde{m}_{e,i}$  = electron and ion mass (kg)

<sup>\*</sup>Graduate Research Assistant, Department of Aerospace Engineering, The University of Texas at Austin.

<sup>&</sup>lt;sup>†</sup>Graduate Research Assistant, Department of Aerospace Engineering, The University of Texas at Austin.

<sup>&</sup>lt;sup>‡</sup>Department of Aerospace Engineering, The University of Texas at Austin.

# **II. Introduction**

Low-temperature nanosecond pulsed discharges have become an object of much study in recent years. The use of short, high voltage pulses are an effective way of generating large electric fields and pulsed capacitive discharges. When a gaseous mixture is exposed to a high electric field, breakdown may occur, and an ionization wave forms and propagates into the gaseous mixture [1]. The streamer eventually forms a plasma conducting channel between the electrodes, which contributes to the generation of active species. The practical interest in nanosecond pulsed discharges is relevant to a variety of applications that include combustion [2-4], water purification [5], and medical technology [6].

Several nanosecond discharge configurations are typically considered. One-dimensional streamer discharges [7] [8] can be representative of a geometry in between parallel electrodes, but the lack of a self-consistent electric field makes the use of two-dimensional and three dimensional models a necessity. Two dimensional simulations between parallel electrodes have been a useful tool to isolate the effect of select parameters [9], or to validate codes [10] due to the simplicity of the applied electric field. However, the study of the formation of a streamer is more realistic when using curved electrode surfaces that induce higher localized electric fields. This led to the use of pin-to-plane geometry [11] for the propagation of a streamer in the direction of the planar surface, and then the pin-to-pin geometry [12] [13] that produces two opposing streamers.

The simulation of nanosecond pulsed discharges presents important numerical challenges. The limiting time scales related to drift, diffusion, ionization, and dielectric relaxation places significant limits on the stable time step size of explicit and semi-implicit time integration schemes. The use of physically accurate boundary conditions [14] that enable the formation of sheaths at the electrodes exacerbates these time step size limitations by requiring finer spatial resolutions and allowing for the formation of larger electric fields. This combination leads to inefficient simulations in more than one dimension that target time scales larger than O(100 ns).

Simulation times of interest that are relevant to the already mentioned practical applications can be of the order of hundreds of microseconds and even milliseconds. Common approaches to relax the limitations of the time integration techniques include simplifying the model during the interpulse phase and/or neglecting the formation of sheaths altogether. While such simplifications might be adequate when studying other important processes that occur away from the electrode surfaces, it can have an impact on the ignition time of both positive and negative streamers, the required voltage to induce the formation and propagation of the streamers, and the shape of the plasma channel. Thus, these simplifications compromise the predictive capability of the model.

In previous work [7] [15], a preconditioned Jacobian-free Newton Krylov method (JFNK) method [16] to solve low-temperature plasma discharges was presented. The approach allows for the efficient simulation of nanosecond discharges with a cathode sheath. In this study, we apply the framework towards a multipulse simulation of an axisymmetric pin-to-pin configuration at atmospheric conditions. The effect of photoionization is approximated with the solution to Helmholtz equations, which allows for the use of a realistic background seed electrons for the first pulse. An overview of the discharge dynamics and time step sizes during each phase of the discharge are presented with this novel framework.

# **III. Governing Equations and Numerical Model**

The plasma fluid model considers the transport of electrons, one species of positive ions, and one species of negative ions. The model used in this study is equivalent to the one presented in previous work [7] [15] and will be summarized below with the addition of photoionization. In this work, dimensional variables are denoted with a tilde, and dimensionless variables are written without the tilde. Air at atmospheric conditions is considered, with a background number density  $\tilde{N}_B$  and background temperature  $\tilde{T}_B$ . Streamer discharges are associated with durations of up to a few hundred nanoseconds, and background properties can be assumed to be constant as long as the discharge does not lead to excessive heating. The governing equations are made dimensionless by choosing a number density  $\tilde{n}_0$ , the Debye length, and the plasma period. When an appropriate number density is chosen, the Debye length is calculated as  $\tilde{\lambda}_0 = \sqrt{\tilde{\epsilon}_0 \tilde{k}_B \tilde{T}_0/\tilde{\epsilon}^2 \tilde{n}_0}$ , where  $\tilde{T}_0$  is a reference temperature,  $\tilde{\epsilon}$  is the unit charge,  $\tilde{\epsilon}_0$  the permittivity in vacuum (unity relative permittivity is assumed), and  $\tilde{k}_B$  is Boltzmann's constant. The plasma period is calculated as  $2\pi/\tilde{\omega}_0$ , where  $\tilde{\omega}_0 = \sqrt{\tilde{\epsilon}^2 \tilde{n}_0/\tilde{\epsilon}_0 \tilde{m}_e}$  is the plasma frequency at reference density  $\tilde{n}_0$ , and  $\tilde{m}_e$  is the electron mass.

The dimensionless electric field vector is

$$\theta = -\nabla \varphi + \mathbf{\Omega},\tag{1}$$

where  $\Omega$  is the electric field resulting from an applied bias voltage to the electrodes and  $\varphi$  is the electrostatic potential associated with space charge, which obeys the Poisson equation

$$-\Delta \varphi = \rho,\tag{2}$$

$$\rho = u - v - n. \tag{3}$$

 $\rho$  is the space charge with u, v, and n indicating the number density of cations, anions, and electrons, respectively, all of them possessing unit charge. The electric field vector has magnitude  $\theta = |\theta|$ . The non-dimensional conservation equation for the electron number density  $n = n(\mathbf{x}, t)$  is

$$\frac{\partial n}{\partial t} = a_1 \nabla \cdot (\theta n) + a_2 T_e \Delta n + \omega_i - \omega_{er} - \omega_a + \omega_d 
= a_1 (\rho n + \theta \cdot \nabla n) + a_2 T_e \Delta n + \omega_i - \omega_{er} - \omega_a + \omega_d + \omega_{\text{ph}},$$
(4)

where  $\mathbf{x}$  is the position vector, t is time, and  $T_e = T_e(\theta)$  is the electron temperature. The contribution of  $\nabla T_e$  to diffusion is neglected, and  $T_e$  is calculated from the electric field consistent with the local-field approximation. The terms  $\omega_i$ ,  $\omega_{er}$ ,  $\omega_a$ , and  $\omega_d$  represent the chemical contribution of ionization, electron-ion recombination, electron attachment, and electron detachment. The term  $\omega_{ph}$  represents the photoionization rate. Further details about this term are presented in Section III.C. The dimensionless transport equations for the number density of positive ions  $u = u(\mathbf{x}, t)$  and negative ions  $v = v(\mathbf{x}, t)$  are given by

$$\frac{\partial u}{\partial t} = -a_7(\rho u + \boldsymbol{\theta} \cdot \nabla u) + a_8 \Delta u + \omega_i - \omega_{er} - \omega_{ir} + \omega_{ph}, \tag{5}$$

$$\frac{\partial v}{\partial t} = a_7(\rho v + \boldsymbol{\theta} \cdot \nabla v) + a_8 \Delta v + \omega_a - \omega_{ir} - \omega_d, \tag{6}$$

where  $\omega_{ir}$  is the chemical contribution of ion-ion recombination. The value of dimensionless parameters  $a_1$ ,  $a_2$ ,  $a_7$ , and  $a_8$  are provided later.

The simplified chemical kinetics model is adapted from the air plasma chemistry model given in

Refs. [11] 17]. The expressions for the chemical sources are calculated

$$\omega_i = r_i n, \tag{7}$$

$$\omega_{er} = (a_5/T_e)un,\tag{8}$$

$$\omega_a = (a_6/T_e)n,\tag{9}$$

$$\omega_{ir} = a_9 v u, \tag{10}$$

$$\omega_d = r_d v. \tag{11}$$

The rate of ionization  $r_i$  is a function of the reduced electric field

$$r_i = \tilde{k}_i (2\pi/\tilde{\omega}_0) \tilde{N}_B, \tag{12}$$

$$\tilde{k}_i = \tilde{f}_i(\tilde{\theta}/\tilde{N}_B),\tag{13}$$

and the functional form of is  $\tilde{k}_i$  is adapted from Ref. [18]. The dimensionless parameters  $a_i$  are provided below

$$a_1 = (2\pi/\tilde{\omega}_0)\tilde{\mu}_e \tilde{N}_B \tilde{\alpha}_0 \tilde{e}/\tilde{\epsilon}_0, \tag{14}$$

$$a_2 = a_1, \tag{15}$$

$$a_3 = (2\pi/\tilde{\omega}_0)\tilde{c}_8^a \tilde{N}_B,\tag{16}$$

$$a_4 = \tilde{c}_8^b \tilde{\epsilon}_0 / (\tilde{e}\alpha_0 \tilde{\lambda}_0), \tag{17}$$

$$a_5 = (2\pi/\tilde{\omega}_0)\tilde{c}_{18}\tilde{n}_0(300/\tilde{T}_0),\tag{18}$$

$$a_6 = (2\pi/\tilde{\omega}_0)\tilde{c}_{19}\tilde{N}_R^2(300/\tilde{T}_0),\tag{19}$$

$$a_7 = (2\pi/\tilde{\omega}_0)\tilde{\mu}_i \tilde{N}_B \alpha_0 \tilde{e}/\tilde{\epsilon}_0, \tag{20}$$

$$a_8 = a_7 \tilde{T}_B / \tilde{T}_0, \tag{21}$$

$$a_9 = (2\pi/\tilde{\omega}_0)\tilde{c}_{22}\tilde{n}_0\tilde{N}_B. \tag{22}$$

The constants appearing in the dimensionless parameters are taken from Refs. [11], 17]:  $\tilde{c}_8^a = 10^{-6} \exp(-8.3 \log 10) = 5.012 \times 10^{-15} \text{ m}^3 \text{ s}^{-1}$ ,  $\tilde{c}_8^b = 8.301 \times 10^{-19} \text{ V m}^2$ ,  $\tilde{c}_{18} = 2 \times 10^{-13} \text{ m}^3 \text{ s}^{-1}$ ,  $\tilde{c}_{19} = 8.82 \times 10^{-43} \text{ m}^6 \text{ s}^{-1}$ , and  $\tilde{c}_{22} = 2 \times 10^{-37} \text{ m}^6 \text{ s}^{-1}$ . The  $r_d$  parameter for electron detachment is approximated as the sum of two components: a weak electric field contribution and a strong electric field contribution taken from Refs. [19] and [20]. The weak field contribution is modeled with the background gas temperature, while the strong electric field contribution is a function of the reduced electric field. The functional form is

$$r_d = \tilde{k}_d (2\pi/\tilde{\omega}_0) \tilde{N}_B,$$
  
$$\tilde{k}_d = 10^{f(\tilde{T})} + 10^{g(\tilde{\theta}/\tilde{N}_B)}.$$

Expressions for  $f(\tilde{T})$  and  $g(\tilde{\theta}/\tilde{N})$  are provided in the Appendix. Constant normalized mobilities are used, with  $\tilde{\mu}_e \tilde{N} = 10^{24} \text{ V}^{-1} \text{ m}^{-1} \text{ s}^{-1}$  and  $\tilde{\mu}_i \tilde{N} = 6.7 \times 10^{21} \text{ V}^{-1} \text{ m}^{-1} \text{ s}^{-1}$ .

# A. Boundary Conditions

Boundary conditions at the cathode are adapted from Gorin et. al. [21]. The boundary conditions include advective and diffusive processes, and secondary emissions in the case of the electrons. Overall, these effects are captured by the Robin boundary condition for the number density of a particle  $\beta$ 

$$-D\frac{\partial \beta}{\partial \zeta} + V\beta = \chi,\tag{23}$$

where D is the diffusion coefficient, V is the Hopf velocity,  $\zeta$  is the local normal coordinate pointing away from the plasma and into the electrode, and  $\chi$  represents particle emissions at the electrode. The secondary emissions are proportional to the secondary emissions coefficient  $\gamma$  [22]. The full details relevant to the implementation are discussed in [7] [15]. A homogeneous Neumann boundary condition is used at the anode for all charged species. In previous numerical experiments, the inclusion of the anode sheath has had a negligible impact during the streamer discharge, although its influence during the interpulse phase has not been assessed. At the axis and the far-field, homogeneous Neumann boundary conditions for all species and the electrostatic potential are used. Finally, Dirichlet boundary conditions for the electrostatic potential are implemented at the electrode surfaces.

### **B.** Discretization

The system of equations is solved as fully coupled and fully implicit with the exception of the photoionization term. A general backward differentiation formula (BDF)

$$\left(\alpha y^{n+1} + \sum_{k=0}^{s-1} C_k y^{n-k}\right) = h f(t^{n+1}, y^{n+1}), \tag{24}$$

is used for the temporal integration of the PDEs. The coefficients  $\alpha$  and  $C_k$  depend on the time step history, and the desired order of accuracy s. Centered finite difference spatial operators of second order are used to approximate the laplacian and gradient operators

$$\Delta y \approx \mathbb{L} y,$$
 (25)

$$\nabla y \approx \mathbb{G}\underline{y},$$
 (26)

and

$$\boldsymbol{\theta} \cdot \nabla y \approx (\boldsymbol{\theta} \cdot \mathbb{G}^{\pm}) \underline{y} = \mathbb{D}^{\pm} \underline{y},$$
 (27)

where y = y(x) is a continuous field and  $\underline{y}$  is the discrete approximation to the continuous field on the finite difference mesh. The system of equations is solved with a preconditioned Jacobian Free Newton Krylov (JFNK) method [16]. The preconditioned strategy is explained in detail in [7] [15].

### C. Photoionization

In the discharge simulations presented in  $\boxed{7.15}$ , the effect of photoionization was neglected. This was a reasonable simplification at the time the numerical methods were developed, since several studies have shown that the effect of photoionization is very limited when the initial level of seed particles is elevated  $\boxed{12}$ , corresponding to charged species number densities of  $O(10^{13} \text{ m}^{-3})$  or higher. However, the effect of photoionization cannot be neglected when the initial level of seed particles is low, as is the case for realistic initial conditions for pin-to-pin discharges prior to the first pulse. For simulations with low amounts of seed particles, the effect of photoionization is crucial for the formation and propagation of streamers.

The simplest model of photoionization requires solving nh Helmholtz equations. Once the solutions to those differential equations are available, their sum is an approximation to the photoionization rate  $\boxed{23}$  Namely

$$\tilde{\omega}_{\rm ph} = \sum_{j}^{nh} \tilde{\omega}_{\rm ph}^{j},\tag{28}$$

$$\tilde{\nabla}^2 \tilde{\omega}_{\rm ph}^j - (\tilde{\lambda}_j \tilde{P}_{\rm O_2})^2 \tilde{\omega}_{\rm ph}^j = -\tilde{A}_j \tilde{P}_{\rm O_2}^2 \tilde{I}(\tilde{\boldsymbol{x}}), \tag{29}$$

and

$$\tilde{I}(\tilde{x}) = \frac{\tilde{P}_q}{\tilde{P} + \tilde{P}_a} \xi \tilde{\omega}_i(\tilde{x}). \tag{30}$$

The fit parameters  $\tilde{\lambda}_j$  [cm<sup>-1</sup>Torr<sup>-1</sup>] and  $\tilde{A}_j$  [cm<sup>-2</sup>Torr<sup>-2</sup>] are selected to reduce approximation errors,  $\tilde{P}_{O_2}$  is the partial pressure of diatomic oxygen,  $\tilde{P}_q$  is the quenching pressure of oxygen, and  $\xi$  an efficiency factor. The model is made dimensionless consistent with reference quantities

$$\nabla^2 \omega_{\rm ph} - B_j^2 \omega_{\rm ph} = -C_j \nu \omega_i(\mathbf{x}),\tag{31}$$

where

$$B_i = \tilde{\lambda}_i \tilde{L}_{\text{ref}}(0.21\tilde{P}_{\text{B}}), \tag{32}$$

$$C_j = \tilde{A}_j \tilde{L}_{\text{ref}}^2 (0.21 \tilde{P}_{\text{B}})^2,$$
 (33)

$$\nu = \frac{\tilde{P}_q}{\tilde{P}_B + \tilde{P}_q} \xi,\tag{34}$$

$$\xi = 0.02,\tag{35}$$

$$\tilde{P}_q = 70 \text{ Torr.} \tag{36}$$

Here,  $\tilde{L}_{ref}$  is equal to the Debye length  $\tilde{\lambda}_0$ , but a different symbol is used to avoid confusion with the Helmholtz equation parameter  $\lambda_j$ . By using these simplifications, the photoionization term becomes a function of the dimensionless ionization rate  $\omega_i$ . Evaluation of the photoionization term  $\omega_{ph}$  requires solving three Helmholtz equations. The fully implicit JFNK formulation requires evaluating the photoionization term at every linear iteration, which can have a significant impact on the efficiency of the solver. As a result, the photoionization term is evaluated explicitly using the extrapolated state at the future time step, and therefore the only term that is not part of the fully implicit formulation. Note that the temporal order of accuracy of the time integration method is maintained because the extrapolation order of accuracy is the same as that of the BDF method. We found that the stability was not compromised by treating the photoionization term explicitly. The values of the Helmholtz equation parameters are presented in Tab. []

Table 1 Parameters for the three term Helmholtz approximation for photoionization from [23]

j	$A_j$ [cm <sup>-2</sup> Torr <sup>-2</sup> ]	$\lambda_j$ [cm <sup>-1</sup> Torr <sup>-1</sup> ]
1	$1.986 \times 10^{-4}$	0.0553
2	0.0051	0.1460
3	0.4886	0.89

# D. Geometry and Setup

In this work, we consider an axisymmetric configuration with a driven parabolic electrode (anode) placed at the top of the domain, separated by a distance H from the bottom parabolic electrode (grounded cathode). The curvature of the electrodes enhances the local electric field, which increases the ionization rates at the tips. If the high electric field is held high for long enough, formation and propagation of opposing streamers ensues [12][13]. After the propagation phase, a conducting channel is formed between the two electrodes. A distinct structure known as the cathode sheath [24] forms near the grounded surface, characterized by low electron number densities, and large electric fields. This structure has an important effect on the simulation

of streamer discharges. First and foremost, it creates a large voltage drop within the sheath that effectively decreases the voltage across the rest of the gap. This effect is difficult to ignore, given that almost every term in the system of partial differential equations depends directly or indirectly on the strength of the electric field. Secondly, due to the high electric fields produced within the region and large gradients in number densities, it introduces significant numerical stiffness. Despite its impact, a substantial number of studies simply neglect the formation of the cathode sheath due to the challenges associated with its modelling.

Nanosecond pulsed discharges over time scales of hundreds of microseconds have been studied in the past 12 25. However, these studies usually neglect electrode sheaths altogether or use a simplified model during the interpulse phase. This study aims to demonstrate the efficiency of a novel fully-implicit JFNK approach over time scales of interest while allowing for the formation of the cathode sheath. A schematic of the configuration is shown in Fig. 1

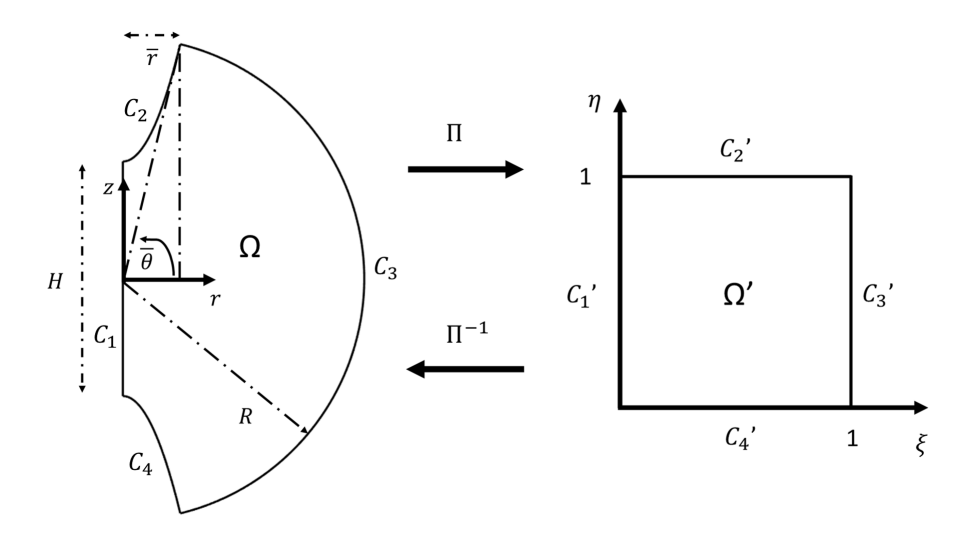


Fig. 1 Schematic of the axisymmetric configuration with the anode at the top, and the electrode surface at the bottom

The computational domain is discretized using curvilinear boundary fitted grids [26], and the parallel finite difference solver is implemented through the Portable, Extensible Toolkit for Scientific Computation (PETSc) [27]. The overall discharge parameters are summarized in Tab. [2] The pin curvature  $\tilde{r}_c$  determines the observed maximum distortion of the electric field around the pins. Frequencies between 10 and 100 kHz are deemed consistent with past experimental studies [28] [29]. A time-varying voltage is applied according to the function

$$\phi(t) = \phi_{max} \left[ \sigma(t - \delta, \lambda) + \sigma(t - \delta - t_p - t_r, -\lambda) - 1 \right], \tag{37}$$

$$\sigma(t,\lambda) = 1/(1 + \exp(-\lambda t)). \tag{38}$$

This function produces a sigmoid profile that imitates one produced by nanosecond pulse voltage generators. A second order BDF method was used for all simulations presented in this work.

Table 2 Configuration parameters for the pin-to-pin discharge.

Geometry		
$ ilde{ ilde{H}}$	0.25 cm	
$ ilde{R}$	0.5 cm	
$ ilde{r}_c$	$150 \mu \mathrm{m}$	
Pulse Parameters		
$ ilde{\phi}_{ ext{max}} \  ilde{t}_p \  ilde{t}_r \  ilde{\delta} \  ilde{\lambda} \  ilde{\lambda}$	10 kV	
$\tilde{t}_p$	2.0 ns	
$\tilde{t}_r$	5 ns	
$ ilde{\delta}$	3.2 ns	
$ ilde{\lambda}$	$8/\tilde{t}_r$	
$ ilde{f}$	50 kHz	
Gas Properties		
$ ilde{T}_B$	300 K	
$ ilde{P}_B$	1 atm	
<b>Cathode Boundary Condition</b>		
$n_{ m em}$	0	
γ	0.01	
Reference Values		
$ ilde{ heta}_0$	10.35 Td	
$\tilde{t}_0$	0.1114 ns	
$\tilde{n}_0$	$10^{18} \text{ m}^{-3}$	
$ ilde{\lambda}_0$	$14.00 \mu \mathrm{m}$	
$ ilde{T_0}$	$4.118 \times 10^4 \text{ K}$	

**IV. Results** 

# A. Discharge Overview

We begin by providing an overview of the discharge dynamics during a nanosecond pulsed discharge featuring multiple pulses. Two-dimensional profiles of the electron number density and reduced electric field are provided in Fig. 2 at various instants. The time instants are selected to coincide with the end of the applied pulse, roughly corresponding to 10 ns after the pulse begins. The number densities are shown in a logarithmic scale, while the reduced electric field is shown on a linear scale.

The applied voltage leads to ionization near the tips, producing opposing streamers. The initial number of seed electrons is low (10<sup>9</sup> m<sup>-3</sup>), and the first 10 kV pulse does not lead to the ignition and connection of the two streamers as shown in the first panel of Fig. 2 During the second pulse, the streamers develop and travel across the preionized path left behind by the initial discharge. The charged species in the preionized path promote faster formation and propagation of streamers, leading to connection and formation of a conducting plasma channel as seen in the second panel of Fig. 2 A similar pattern is seen during the third, and fourth pulses where streamers develop, travel through the preionized path, connect and form a plasma channel, and then diffuse after the pulse ends. The two-dimensional profiles are complemented by the maximum electron and ion number densities provided in Fig. 3

Peak number densities increase rapidly once the applied voltage pulse begins, which corresponds to the first steep rise observed in Fig.  $\boxed{3}$  The second steep rise corresponds with the time of streamer connection, which is absent from the first pulse. Positive ions and electrons reach a maximum number density of approximately  $4 \times 10^{20}$  m<sup>-3</sup>, while the maximum number of negative ions remains an order of magnitude lower. The applied voltage decreases at 10 ns after the pulsing period begins and populations of electrons

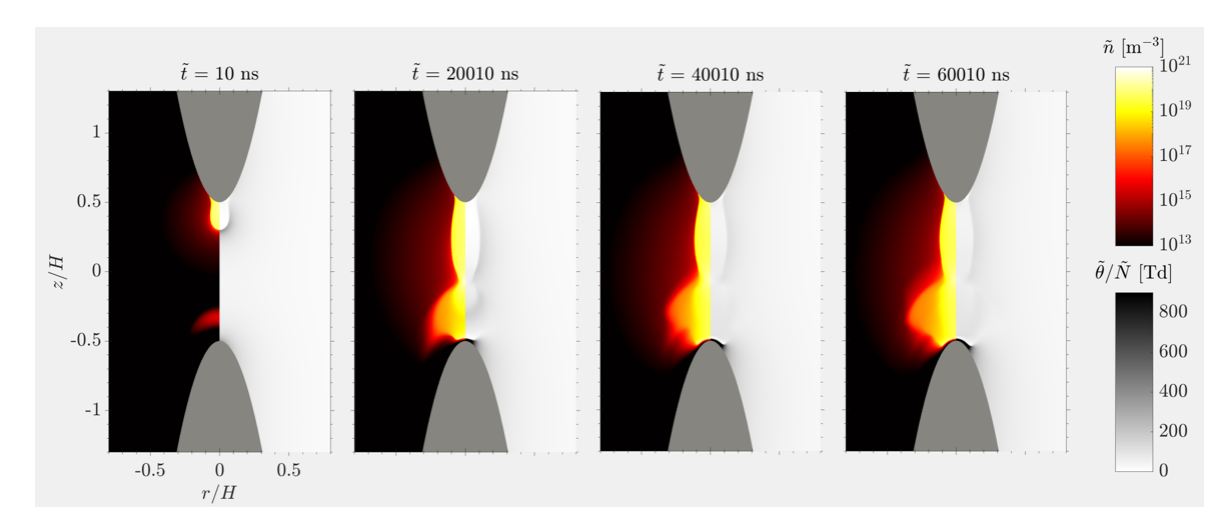


Fig. 2 Electron number densities (left side of each panel) and reduced electric field magnitude (right side of each panel) at four different instants in time corresponding to four pulses.

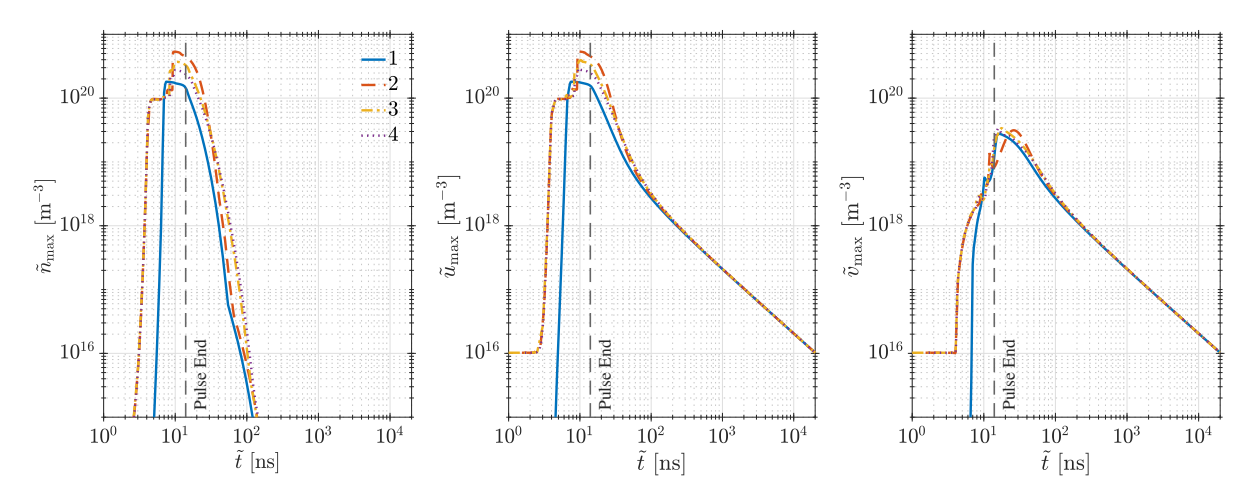


Fig. 3 Maximum number densities as a function of time for electrons (left panel), positive ions (center panel), and negative ions (right panel)

remain relatively high for about 100 ns, before diffusion and recombination lead to a significant reduction in the concentration of electrons throughout the channel. Important concentrations of positive and negative ions persist over much longer time scales, with the ionized channel produced by the streamer remaining at number densities of  $10 \times 10^{16}$  m<sup>-3</sup> by the time the next pulse strikes.

After the first pulse, the maximum number densities display a remarkable periodicity during the streamer propagation phase, although there are noticeable differences directly after streamer connection. Despite these differences, the maximum number densities observed in the channel remain the same at the end of the pulsing period. Notice that the maximum number densities are consistent with those of a glow type discharge 12 28 29, which result in moderate heating of the background gas. Note that in these simulations the background gas temperature and pressure are assumed to remain constant. Longer or stronger voltage pulses, or significantly larger pulsing frequencies would result in plasma densities that are more representative of an spark or arc regime. For a spark or arc discharge, there is significant gas heating that requires a more complex physical model accounting for changes to the thermochemical state of the background gas.

#### B. Time scales

Our novel fully-implicit time integration method to step over the most stringent limiting time scales corresponding to drift, diffusion, dielectric, and ionization processes with the inclusion of the cathode sheath is a key enabling technology for the simulation of nanosecond pulsed discharges. The time step size and limiting time scales corresponding to the second pulse are shown in Fig. 4 using a minimum spatial grid spacing of 1.25  $\mu$ m, resulting in 1.68 M grid points. An adaptive time step size strategy with error estimation is used to ensure a relative tolerance of  $10^{-3}$ , but time steps are not rejected to maintain efficient use of resources. Four pulses were simulated over a wall-clock time of 10 hrs using 224 processors over 4 computational nodes on the supercomputer Frontera at the Texas Advanced Computing Center (TACC).

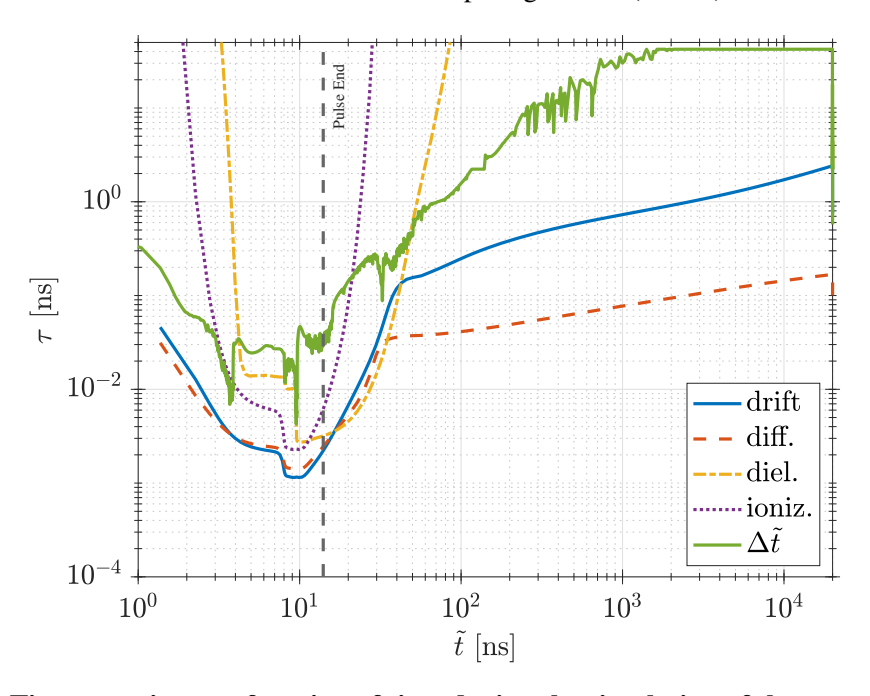


Fig. 4 Time step size as a function of time during the simulation of the second pulse

Fig. 4 shows that as the applied voltage increases, so does the electric field which leads to a steady decrease in the limiting time scales due to ionization, diffusion, and drift. The limiting time scales drops to 1 ps while the voltage is applied. After the pulse ends, the maximum electric field decreases rapidly, and the dielectric scale becomes the most limiting time scale (about O(10 ps)) for around 30 ns. The number density of electrons then decreases due to diffusion and recombination, and the diffusive time scale becomes the most limiting time scale for the rest of the interpulse period. The implicit time stepping strategy allows to step over all such time scales at one point or another, while retaining a user defined relative accuracy of  $10^{-3}$ . The time step sizes are between 10 and 30 ps during the applied pulse and increase steadily to the user-defined maximum of 40 ns.

#### V. Conclusions

A novel preconditioned Jacobian-free Newton Krylov solver with fully-implicit time stepping was used to simulate nanosecond pulsed glow discharges in an axisymmetric pin-to-pin configuration. The plasma fluid model with drift-diffusion is applied to electrons, one species of positive ion, and one species of negative ion using the local-field approximation. A simplified kinetics model that includes ionization, electron and ion recombination, and electron attachment, and detachment was utilized. Photoionization was approximated with the solution to three Helmholtz equations and it was the only component of the model that is integrated explicitly in time without any adverse effects on stability. Finally, realistic boundary conditions were utilized to allow for the formation of a cathode sheath.

The application of multiple voltage pulses led to the formation and propagation of opposing streamers at every pulse. In the first pulse, the initial level of electrons was insufficient for streamer connection for this particular pulse strength. During subsequent pulses, the preionized path left from previous pulses contributed to streamers closing the gap and forming a conducting plasma channel during every pulse thereafter. A periodic pattern quickly developed, although noticeable differences were seen after the streamer connection during each pulse.

The stiffness encountered during all phases of the discharge is typically a major roadblock to traditional implementations using explicit and semi-implicit methods. A coupled implicit method allowed the solver to step over all the stiff time scales, including electron drift and diffusion processes, dielectric relaxation, and ionization. Temporal accuracy was ensured by an adaptive time step strategy with error estimation and imposing a user defined relative tolerance of  $10^{-3}$ . The longer time steps combined with the efficiency of the JFNK solver enabled simulations over tens of microseconds corresponding to a pulsing frequency of 50 kHz.

# A. Appendix

# A. Detachment functional fits

The dimensional detachment rate constant is given by

$$\tilde{k}_d = 10^{f(\tilde{T})} + 10^{g(\tilde{\theta}/\tilde{N}_B)} \text{ [cm}^3/\text{s]},$$

where the temperature dependent component  $f(\tilde{T})$  is a second order polynomial and the component that depends on the reduced electric field  $f(\tilde{\theta}/\tilde{N}_R)$ , is a fourth order polynomial. Expressions for the fits are

$$\begin{split} f(\tilde{T}) &= c_{d1}\tilde{T}^2 + c_{d2}\tilde{T} + c_{d3}, \\ g(\tilde{\theta}/\tilde{N}) &= c_{d4}(\tilde{\theta}/\tilde{N})^4 + c_{d5}(\tilde{\theta}/\tilde{N})^3 + c_{d6}(\tilde{\theta}/\tilde{N})^2 + c_{d7}(\tilde{\theta}/\tilde{N}) + c_{d8}, \\ c_{d1} &= -2.026 \text{x} 10^{-5}, \\ c_{d2} &= 3.062 \text{x} 10^{-2}, \\ c_{d3} &= -2.470 \text{x} 10^1, \\ c_{d4} &= -1.319 \text{x} 10^{-9}, \\ c_{d5} &= 1.305 \text{x} 10^{-6}, \\ c_{d6} &= -4.818 \text{x} 10^{-4}, \\ c_{d7} &= 8.344 \text{x} 10^{-2}, \\ c_{d8} &= -1.653 \text{x} 10^1. \end{split}$$

The polynomials are fit to the data shown in Fig. 2 in [19] and Fig. 11 in [20]

#### References

- [1] Nijdam, S., Teunissen, J., and Ebert, U., "The physics of streamer discharge phenomena," *Plasma Sources Sci. Technol.*, Vol. 29, 2020.
- [2] Ju, Y., and Sun, W., "Plasma assisted combustion: Dynamics and chemistry," *Prog. Energy and Combust. Sci.*, Vol. 48, 2015, pp. 21–83.
- [3] Starikovskii, A. Y., Nikipelov, A., Nudnova, M., and Roupassov, D., "SDBD plasma actuator with nanosecond pulse-periodic discharge," *Plasma Sources Sci. Technol.*, Vol. 18, No. 3, 2009, p. 034015.
- [4] Deak, N., Bellemans, A., and Bisetti, F., "Plasma-assisted ignition of methane/air and ethylene/air mixtures: Efficiency at low and high pressures," *Proc. Combust. Inst.*, 2020.
- [5] Akiyama, H., "Streamer discharges in liquids and their applications," *IEEE Trans. Dielectr. Electr. Insul.*, Vol. 7, No. 5, 2000, pp. 646–653.
- [6] Nastuta, A. V., Topala, I., Grigoras, C., Pohoata, V., and Popa, G., "Stimulation of wound healing by helium atmospheric pressure plasma treatment," *J. Phys. D: Appl. Phys.*, Vol. 44, No. 10, 2011, p. 105204.
- [7] Duarte, A. J., Deak, N., and Bisetti, F., "One-Dimensional Streamer Simulations Using a Jacobian Free Newton-Krylov Method with Physics Based Preconditioning," *AIAA Scitech 2022 Forum*, 2022.
- [8] Davies, A., Evans, C., and Jones, F. L., "Electrical breakdown of gases: the spatio-temporal growth of ionization in fields distorted by space charge," *Proc. R. Soc. Lond. Series A. Mathematical and Physical Sciences*, Vol. 281, No. 1385, 1964, pp. 164–183.
- [9] Georghiou, G. E., Morrow, R., and Metaxas, A. C., "The effect of photoemission on the streamer development and propagation in short uniform gaps," *J. Phys. D: Appl. Phys.*, Vol. 34, No. 2, 2000, pp. 200–208.
- [10] Bagheri, B., Teunissen, J., Ebert, U., Becker, M. M., Chen, S., Ducasse, O., Eichwald, O., Loffhagen, D., Luque, A., Mihailova, D., Plewa, J. M., van Dijk, J., and Yousfi, M., "Comparison of six simulation codes for positive streamers in air," *Plasma Sources Sci. Technol.*, Vol. 27, No. 9, 2018, p. 095002.
- [11] Pancheshnyi, S. V., and Starikovskii, A. Y., "Two-dimensional numerical modelling of the cathode-directed streamer development in a long gap at high voltage," *J. Phys. D: Appl. Phys.*, Vol. 36, 2003, pp. 2683–2691.
- [12] Tholin, F., and Bourdon, A., "Simulation of the stable 'quasi-periodic' glow regime of a nanosecond repetitively pulsed discharge in air at atmospheric pressure," *Plasma Sources Sci. Technol.*, Vol. 22, No. 4, 2013, p. 045014.
- [13] Zhang, A., Scarcelli, R., Wallner, T., Breden, D., Karpatne, A., Raja, L. L., Ekoto, I., and Wolk, B., "Numerical investigation of nanosecond pulsed discharge in air at above-atmospheric pressures," J. Phys. D: Appl. Phys., Vol. 51, 2018.
- [14] Wilson, A., and Shotorban, B., "Investigation of surface boundary conditions for continuum modeling of RF plasmas," *Phys. Plasmas*, Vol. 25, 2018.
- [15] Duarte Gomez, A., Deak, N., and Bisetti, F., "Jacobian-free Newton–Krylov method for the simulation of non-thermal plasma discharges with high-order time integration and physics-based preconditioning," *J. of Comput. Phys. (under review)*, 2023.
- [16] Knoll, D., and Keyes, D., "Jacobian-free Newton–Krylov methods: a survey of approaches and applications," *J. Comput. Phys.*, Vol. 193, No. 2, 2004, pp. 357–397.
- [17] Kossyi, I. A., Kostinsky, A. Y., Matveyev, A. A., and Silakov, V. P., "Kinetic scheme of the non-equilibrium discharge in nitrogen-oxygen mixtures," *Plasma Sources Sci. Technol.*, Vol. 1, 1992, p. 207.
- [18] Morrow, R., and Lowke, J. J., "Streamer propagation in air," *J. Phys. D: Appl. Phys.*, Vol. 30, No. 4, 1997, pp. 614–627.

- [19] Aleksandrov, N. L., and Anokhin, E. M., "Electron detachment from O2 ions in oxygen: the effect of vibrational excitation and the effect of electric field," *J. Phys. B*, Vol. 44, No. 11, 2011, p. 115202.
- [20] Ponomarev, A. A., and Aleksandrov, N. L., "Monte Carlo simulation of electron detachment properties for O2ions in oxygen and oxygen:nitrogen mixtures," *Plasma Sources Sci. Technol.*, Vol. 24, No. 3, 2015, p. 035001.
- [21] Gorin, V., Kudryavtsev, A., Yao, J., Yuan, C., and Zhou, Z., "Boundary conditions for drift-diffusion equations in gas-discharge plasmas," *Phys. Plasmas*, Vol. 27, No. 1, 2020, p. 013505.
- [22] Belasri, A., Boeuf, J. P., and Pitchford, L. C., "Cathode sheath formation in a discharge-sustained XeCl laser," *J. Appl. Phys.*, Vol. 74, No. 3, 1993, pp. 1553–1567.
- [23] Bourdon, A., Pasko, V. P., Liu, N. Y., Célestin, S., Ségur, P., and Marode, E., "Efficient models for photoionization produced by non-thermal gas discharges in air based on radiative transfer and the Helmholtz equations," *Plasma Sources Sci. Technol.*, Vol. 16, 2007, pp. 656–678.
- [24] Franklin, R. N., "The plasma-sheath boundary region," *J. Phys. D: Appl. Phys.*, Vol. 36, No. 22, 2003, pp. R309–R320.
- [25] Niknezhad, M., Chanrion, O., Kahn, C., Holbøll, J., and Neubert, T., "A three-dimensional model of streamer discharges in unsteady airflow," *Plasma Sources Sci. Technol.*, Vol. 30, No. 4, 2021, p. 045012.
- [26] Thompson, J. F., Thames, F. C., and Mastin, C., "Automatic numerical generation of body-fitted curvilinear coordinate system for field containing any number of arbitrary two-dimensional bodies," *J. Comput. Phys.*, Vol. 15, No. 3, 1974, pp. 299–319.
- [27] Balay, S., Abhyankar, S., Adams, M. F., Benson, S., Brown, J., Brune, P., Buschelman, K., Constantinescu, E., Dalcin, L., Dener, A., Eijkhout, V., Gropp, W. D., Hapla, V., Isaac, T., Jolivet, P., Karpeev, D., Kaushik, D., Knepley, M. G., Kong, F., Kruger, S., May, D. A., McInnes, L. C., Mills, R. T., Mitchell, L., Munson, T., Roman, J. E., Rupp, K., Sanan, P., Sarich, J., Smith, B. F., Zampini, S., Zhang, H., Zhang, H., and Zhang, J., "PETSc/TAO Users Manual," Tech. Rep. ANL-21/39 Revision 3.15, Argonne National Laboratory, 2022.
- [28] Pai, D. Z., Stancu, G. D., Lacoste, D. A., and Laux, C. O., "Nanosecond repetitively pulsed discharges in air at atmospheric pressure The glow regime," *Plasma Sources Sci. Technol.*, Vol. 18, 2009.
- [29] Pai, D. Z., Lacoste, D. A., and Laux, C. O., "Transitions between corona, glow, and spark regimes of nanosecond repetitively pulsed discharges in air at atmospheric pressure," *J. Appl. Phys.*, Vol. 107, 2010.